*Mineralogical Magazine, August 2004, Vol. 68(4), pp. 649–667*

# A new graphical presentation and subdivision of potassium micas

G. TISCHENDORF[1], M. RIEDER[2], H.-J. FÖRSTER[3,*], B. GOTTESMANN[4] AND CH. V. GUIDOTTI[5]

[1] Bautzner Straße 16, D-02763 Zittau, Germany
[2] Department of Geochemistry, Mineralogy, and Mineral Resources, Charles University, Albertov 6, CZ-12843 Praha 2, Czech Republic
[3] Institute of Earth Sciences, University of Potsdam, P.O. Box 601553, D-14415 Potsdam, Germany
[4] GeoForschungsZentrum Potsdam, Telegrafenberg, D-14473 Potsdam, Germany
[5] Department of Geological Sciences, University of Maine, Orono, ME 04469-5790, USA

**ABSTRACT**

A system based on variation of the octahedrally coordinated cations is proposed for graphical presentation and subdivision of tri- and dioctahedral K micas, which makes use of elemental differences (in a.p.f.u.): (Mg − Li) [= *mgli*] and ($Fe_{tot}$ + Mn + Ti − $^{VI}$Al) [= *feal*]. All common true tri- and dioctahedral K micas are shown in a single polygon outlined by seven main compositional points forming its vertices. Sequentially clockwise, starting from $Mg_3$ (phlogopite), these points are: $Mg_{2.5}Al_{0.5}$, $Al_{2.167}\square_{0.833}$, $Al_{1.75}Li_{1.25}$, $Li_2Al$ (polylithionite), $Fe^{2+}_2Li$, and $Fe^{2+}_3$ (annite). Trilithionite ($Li_{1.5}Al_{1.5}$), $Li_{1.5}Fe^{2+}Al_{0.5}$, $Fe^{2+}_2Mg$, and $Mg_2Fe^{2+}$ are also located on the perimeter of the polygon. IMA-siderophyllite ($Fe^{2+}{}_2Al$) and muscovite ($Al_2\square$) plot inside.

The classification conforms with the IMA-approved mica nomenclature and differentiates among the following mica species according to their position in a diagram consisting of *mgli* and *feal* axes plotted orthogonally; trioctahedral: phlogopite, biotite, siderophyllite, annite, zinnwaldite, lepidolite and tainiolite; dioctahedral: muscovite, phengite and celadonite. Potassium micas with [Si] <2.5 a.p.f.u. including IMA-siderophyllite, $KFe^{2+}_2AlAl_2Si_2O_{10}(OH)_2$, and IMA-eastonite, $KMg_2AlAl_2Si_2O_{10}(OH)_2$ seem not to form in nature.

The proposed subdivision has several advantages. All common true, trioctahedral and dioctahedral K micas, whether Li-bearing or Li-free, are shown within one diagram, which is easy to use and gives every mica composition an unambiguously defined name. Mica analyses with $Fe^{2+}$, $Fe^{3+}$, $Fe^{2+}$ + $Fe^{3+}$, or $Fe_{tot}$ can be considered, which is particularly valuable for microprobe analyses. It facilitates easy reconstruction of evolutionary pathways of mica compositions during crystallization, a feature having key importance in petrologically oriented research. Equally important, the subdivision has great potential for understanding many of the crystal-chemistry features of the K micas. In turn this may allow one to recognize and discriminate the extent to which crystal chemistry or bulk composition controls the occurrence of some seemingly possible or hypothetical K mica.

**KEYWORDS:** K micas, trioctahedral, dioctahedral, celadonite, classification.

## Introduction

POTASSIUM micas are widespread in endogenous (magmatic, metamorphic, hydrothermal) rocks and constitute the most important mica group on earth. Their extended compositional variability makes K micas difficult to classify, and various approaches have been published in the literature. Most classifications considered the occupancy of the octahedral sheet (e.g. Foster, 1960*a*,*b*), which is composed of at least four essential cations (Al, Fe, Mg, Li) that are able to replace one another. Whereas the octahedral sheets of mica end-members (formulas recalculated to $22^+$-cation charges) contain only one or two elements (e.g. phlogopite [$Mg_3$], annite [$Fe^{2+}_3$], muscovite [$Al_2\square$], polylithionite [$Li_2Al$]), natural micas

* E-mail: for@geo.uni-potsdam.de
DOI: 10.1180/0026461046840210

typically are members of solid-solution series and contain three or more octahedral cations, i.e. biotite [$Fe^{2+}_{1.5}MgAl_{0.5}$], siderophyllite [$Fe^{2+}_{1.75}Al_{0.75}Mg_{0.25}Li_{0.25}$], zinnwaldite [$Al_{1.25}LiFe^{2+}_{0.25}\square_{0.5}$], phengite [$Al_{1.25}Mg_{0.5}Fe^{2+}_{0.25}\square$], or Li-Fe-bearing muscovite [$Al_{1.625}Li_{0.5}Fe^{2+}_{0.125}\square_{0.75}$].

The recent mica classification, elaborated by the International Mineralogical Association (IMA) Commission on New Minerals and Mineral Names (CNMMN) Mica Subcommittee, considers the main principles of mineral nomenclature (Rieder *et al*., 1998). It was not compiled solely in the context of the mica group, but was a part of the IMA's desire to eliminate unnecessary names. Hence, it had to follow principles that could be applied to all mineral groups. Rieder *et al*. (1998) list valid end-member formulae for trioctahedral and dioctahedral micas and typical compositional ranges for some dioctahedral species. Although this nomenclature is straightforward for compositions close to the end-members, classifying real solid-solution members becomes complicated. Because micas, as a rule, are distinguished by poly-dimensional substitutions, the IMA 50/50%-rule is difficult to apply. In view of the genetic importance and potential for recognizing rock-forming conditions and evolutionary paths, a more detailed classification with clearly defined mineral names and boundaries was desirable.

In this context, we propose a specialized, descriptive subdivision scheme of common true K micas based on the octahedral occupancy expressed by the parameters (Mg − Li) and ($Fe_{tot}$ + Mn + Ti minus $^{VI}Al$). The essential features of this classification have already been presented by Tischendorf *et al*. (1997) and applied to various purposes (Tischendorf *et al*., 1999, 2001*a*,*b*; Yavuz, 2001, 2003*a*,*b*). The following proposal is an effort to strike a compromise between the approach of Tischendorf *et al*. (1997) and that advocated by the IMA Commission on New Minerals and Mineral Names (Nickel and Grice, 1998) and its Mica Subcommittee (Rieder *et al*., 1998). This subdivision provides a solid platform for assessing the crystallochemical, petrological and geological factors, which control what K micas can occur in nature and with what compositional ranges.

## Historical background of K-mica classification

The classification of the micas has received considerable attention over the past 50 years (e.g. Heinrich, 1946; Foster, 1960*a*,*b*; Tröger, 1962; Rieder, 1970; Koval' *et al*., 1972; Gottesmann and Tischendorf, 1978; Černý and Burt, 1984; Monier and Robert, 1986; Burt, 1991; Rieder *et al*., 1998; Sun and Yu, 1999, 2000). Previous approaches typically used either triangular projections or *n*-dimensional vector graphics. Triangular projections make use of relative proportions rather than absolute quantities, which sometimes may be a liability. Although universal in scope, n-dimensional systems may be difficult to visualize. Usually they are poorly arranged, complicated to interpret and, therefore, unsuitable for classifying the micas quickly, especially for non-specialists. Classifications dealing only with either Mg-bearing or Li-bearing micas will misclassify, or inadequately classify, micas with both substantial Mg and Li. Condensing $Fe^{2+}$ and Mg does not meet petrological requirements. Separate classifications for trioctahedral or dioctahedral micas are particularly problematical for description of species that are in-between, i.e. the so-called transitional micas. Many of the drawbacks of previous mica classifications are overcome by the present proposal.

### *The subdivision scheme*

#### *Underlying assumptions*

This proposal only considers K micas, but it can readily be extended to include the Na, Ca and Ba micas. The scheme has been explored for common true K micas and not for those containing unusual elements as major constituents such as Mn (masutomilite, norrishite, montdorite), Zn (hendricksite), V (roscoelite) or Cr (chromphyllite). However, we have to comment on the exotic mica tainiolite [$Mg_2Li$] as well as on micas of the celadonite group [$Al_{0.5}Fe^{3+}_{0.5}Fe^{2+}_{0.5}Mg_{0.5}\square$], because their octahedral sheets are made up of the essential elements upon which the proposal is based.

### *Principle of the diagram*

The diagram should accommodate the following requirements for most widespread application: (1) inclusion of trioctahedral and dioctahedral micas; (2) treatment of Mg and Li micas; (3) uncondensed representation of $Fe^{2+}$ and Mg in micas; and (4) presentation in two-dimensional space.

Because the K micas are so compositionally variable, their presentation and subdivision demands a reduction of the number of variables.

Previous approaches have used three variables (Burt, 1991) or four (if $Fe^{2+}$ and Mg are treated separately) or even seven components (Sun and Yu, 1999) to present micas. Occupancy of the tetrahedral sheet is strictly related to occupancy of the octahedral sheet, because the sum of charges of the tetrahedrally and octahedrally coordinated cations is constant and equals 21. Therefore, it is sufficient to consider only cations substituted in the octahedral sheet (Ti, $^{VI}$Al, $Fe^{3+}$, $Fe^{2+}$, Mg, Mn, Li) for presentation and classification.

These seven cations in the octahedral sheet were further reduced to four. Titanium (assumed to be mostly octahedrally coordinated; see Zhang *et al*., 1993) and Mn are added to Fe because of their geochemically analogous behaviour (see Tischendorf *et al*., 1997, p. 822ff). Iron is expressed as $Fe_{tot}$, i.e. no discrimination is made between $Fe^{3+}$ and $Fe^{2+}$. This simplification introduces some inaccuracy in the total positive charges, but it opens up the applicability of the system to analyses of micas with Fe in either valence state or with total iron undifferentiated (electron-microprobe analyses). The effect of totalling Fe appears to have only a minimal effect on the numerical values of *mgli* and *feal*, with the exception of celadonitic micas (see discussion below).

The strongly antithetical behaviour between Mg and Li (with the exception of tainiolite) (see Tischendorf *et al*., 1997, their Fig. 4*f*), and between $^{VI}$Fe and $^{VI}$Al, in the micas permits these four components to be reduced to two, by using their respective differences (a.p.f.u.): (Mg − Li) [= *mgli*] and ($Fe_{tot}$ + Mg + Ti − $^{VI}$Al) [= *feal*]. This manipulation is unconventional for the representation of minerals, but it results in a data reduction required to describe in two dimensions a complex chemical system. Both parameters represent exchange vectors in the sense of Bragg (1937) and Thompson (1982). Černý and Burt (1984) were the first to utilize this approach for the description of the compositional variation in the mica system. The parameter *mgli* can be considered as being equivalent to $Mg[2Li]_{-1}$ and thus is to be regarded as a reduced expression of $3Mg^{IV}Al[2Li^{VI}AlSi]_{-1}$. The parameter *feal* stands for a reduced expression of $3Fe^{2+}[2^{VI}Al]_{-1}$. The variables *mgli* and *feal* both vary from 3 to −2 (*feal* up to −2.167), thereby covering the whole range of compositional variation of the tri- and dioctahedral micas.

To characterize K micas completely, knowledge of their Li abundance is essential (e.g. Rieder, 2001). Ignoring Li is one of the main causes for misclassification of micas. If not determined directly by SIMS or conventional techniques using mineral separates, various numerical approaches for indirect Li determination have been published, which provide fairly good estimates for the bulk of K micas (Tischendorf *et al*., 1997, 1999, and references therein). A compilation of the most recommended empirical equations for calculation of Li in micas formed in various geological environments is given in the Appendix.

### *Position of K mica end-members and ideal members in the diagram*

Figure 1 shows the position of IMA-confirmed mica end-members and other ideal members essential for describing the K-mica system in the *mgli-feal* diagram. The outer boundary of the polygon is defined by micas with the maximum octahedral occupancy in terms of (Mg + $Fe_{tot}$ + Mn + Ti + Li + $^{VI}$Al), which concomitantly fulfil the $22^+$-charges-per-formula-unit condition, irrespective of their Si/$^{IV}$Al ratio (see the following section).

The diagram offers a prediction of micas not yet known from nature. In the Li-Fe mica subgroup, an Fe-rich composition can be conceived with the theoretical formula $KFe^{2+}_2LiSi_4O_{10}F_2$, [= member $Fe^{2+}_2$Li: *mgli* = −1; *feal* = 2; hereafter abbreviated as coordinates (−1;2)], which is not known to occur in nature. This mica, here referred to as 'Al-free zinnwaldite', corresponds to "Fe-tainiolite" of Černý and Burt (1984, their Fig. 7). Halfway along the line connecting the $Fe^{2+}_2$Li member with $Li_2Al$ (polylithionite, Fig. 1), a trilithionite-like mica with the theoretical formula $K\ Li_{1.5}Fe^{2+}Al_{0.5}Si_4O_{10}F_2$ (−1.5;0.5) is plotted. Our calculations also argue for the existence of dioctahedral K micas richer in Al than muscovite yet fulfilling the $22^+$-charge condition. Such Al-rich micas would have compositions $KAl_{2.5}\square_{0.5}Al_{2.5}Si_{1.5}O_{10}(OH)_2$ at (0;−2.5) or $KAl_3Al_4O_{10}(OH)_2$ at (0;−3). The latter 'mica' contains Al as the only cation in tetrahedral coordination and here is referred to as "hyper-muscovite". One can even theoretically calculate Li or Mg-bearing formula compositions such as $KLi_{0.5}Al_{2.5}Al_3SiO_{10}(OH)_2$ or $KMg_{0.5}Al_{2.5}Al_{3.5}Si_{0.5}\ O_{10}(OH)_2$. Note that in the lower segment of the polygon with [Si] <2.5 (or Si/$^{IV}$Al <1.67), $^{VI}R$ increases from 2.17 to 3, corresponding to a change in the crystal structure from dioctahedral to trioctahedral.

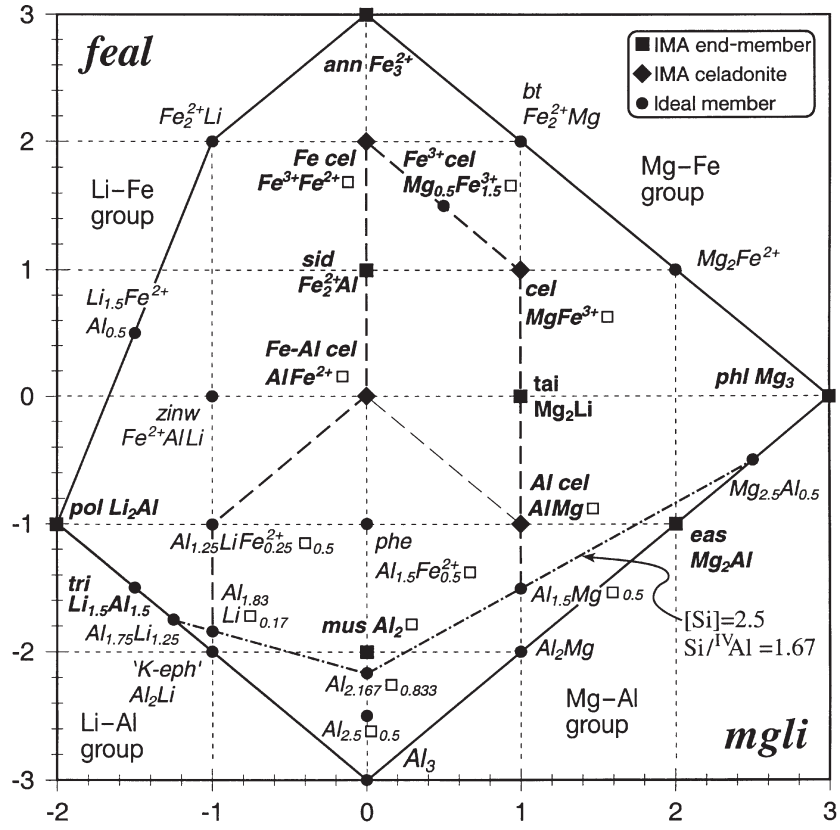


FIG. 1. End-members and ideal members of common K micas plotted in terms of *mgli vs. feal* (in a.p.f.u.). The polygon encloses all possible micas fulfilling the $22^+$-charge condition. Al cel: aluminoceladonite, ann: annite, bt: biotite, cel: celadonite, eas: eastonite, Fe-Al cel: ferro-aluminoceladonite, Fe cel: ferroceladonite, $Fe^{3+}$cel: ferriceladonite, 'K-eph': K-ephesite, mus: muscovite, phe: phengite, phl: phlogopite, pol: polylithionite, sid: siderophyllite, tai: tainiolite, tri: trilithionite, zinw: zinnwaldite. IMA end-members are emphasized using larger symbols. The [Si] isoline is shown (identical with $Si/^{IV}Al$), which divides the area with [Si] >2.5 (or $Si/^{IV}Al$ >1.67) (above) from that with [Si] <2.5 (or $Si/^{IV}Al$ <1.67) (below).

### *Occupancy of the tetrahedral sheet*

The bulk of the 3500 natural mica compositions evaluated in this study have 2.5−3.8 Si a.p.f.u., corresponding to $Si/^{IV}Al$ ratios between 1.67 and 19 in the tetrahedral sheet (Fig. 2). A plot of fixed values or ranges of [Si] as a function of *mgli* and *feal* shows that micas with [Si] <2.5 do not occur in nature. Lithium-rich trioctahedral micas (i.e. near-polylithionite and the $Fe_2^{2+}Li$ member) are distinguished by [Si] between 3.5 and 4. Several IMA end-member micas (phl, ann, mus, tri) and ideal compositions at the tieline phl-ann are characterized by [Si] = 3. A certain [Si] minimum is observed near *mgli* = 0 and *feal* = +2 to −0.5 as well as parallel to the phl-ann tieline. Areas related to tainiolite and the celadonites (not shown in Fig. 2) are distinguished by [Si] near 4, that means $Si/^{IV}Al$ ratios near infinity (see Tables 1 and 2).

Micas of the most Al-rich sector of the diagram (*feal* <−2) bear characteristically low [Si] contents. A line corresponding to [Si] = 2.5 (or $Si/^{IV}Al$ = 1.67) seems to mark a lower limit for naturally occurring micas on the *mgli-feal* diagram. Accordingly, the theoretically most Al-rich mica should have a formula of $KAl_{2.167}\square_{0.833}Al_{1.5}Si_{2.5}(OH)_2$ (0;−2.167) (hereafter termed "trans-muscovite"). [Si] of "trans-muscovite" (2.5) is much lower than that of the IMA end-member muscovite (3.0). The lowest [Si] content of muscovites in our database is equal to 2.9.

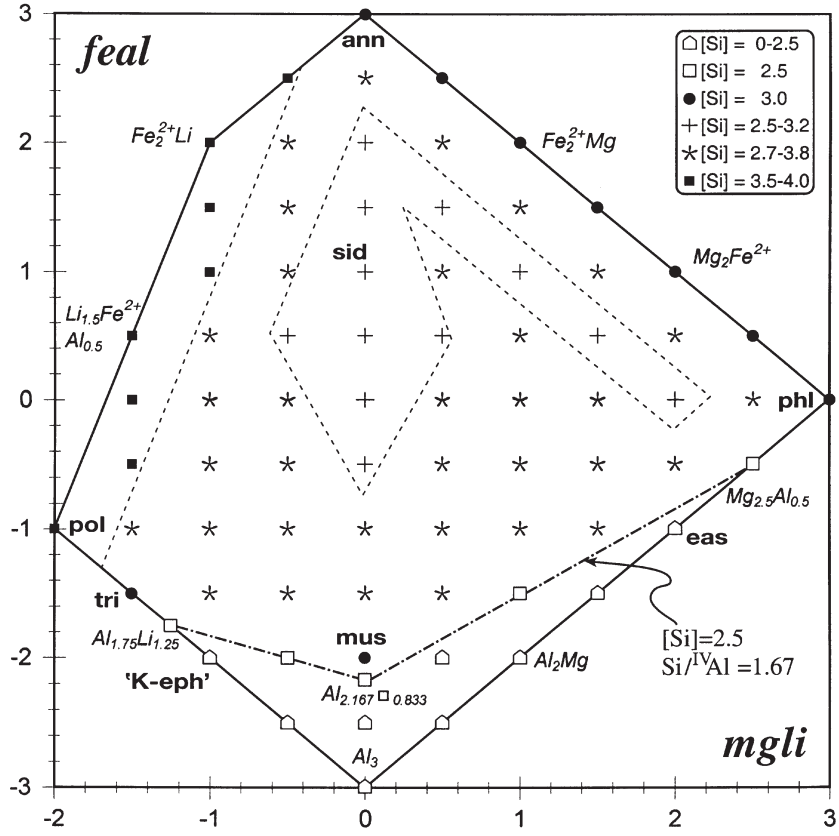


FIG. 2. Occupancy of the tetrahedral sheet by [Si] for common K micas corresponding to $XY_{2-3}Z_4O_{10}(OH,F)_2$ (excluding tainiolite and $Fe^{3+}$-bearing celadonites) plotted on the *mgli–feal* grid. [Si] intervals and one [Si] isoline are shown dividing the area with [Si] >2.5 (above) from that with [Si] <2.5 (below). The only exception is the IMA siderophyllite with [Si] = 2 for *mgli* = 0 and *feal* = 1. Abbreviations as in Fig. 1.

### *Occupancy of the octahedral sheet*

Figure 3 represents the distribution of the octahedral occupancy for ideal K-mica species ($^{VI}R$) as a function of *mgli* and *feal*. Trioctahedral micas with a theoretically high octahedral occupancy ($^{VI}R$ = 3) concentrate along the margins of the diagram, and especially in the area near polylithionite and the $Fe_2^{2+}Li$ member. Trioctahedral micas with an octahedral occupancy between 3 and 2.5 occupy a relatively large portion of the diagram (*mgli* from −1 to 1.5; *feal* >0.5). Dioctahedral micas ($^{VI}R$ <2.5) cluster in a limited area (*mgli* from −0.5 to 1; but *feal* =0), with ideal muscovite (0;−2) at its bottom. An area for micas with $^{VI}R$ = 2.5−2.25 forms a crescent-shaped region that surrounds the field of micas with $^{VI}R$ = <2.25. Intermediate micas with $^{VI}R$ ≈2.5 are positioned between trioctahedral and dioctahedral mica areas. In the *mgli-feal* diagram the line [Si] = 2.5 (corresponding to $Si/^{IV}Al$ = 1.67) is the outer boundary of the field containing natural K micas. This line intersects several $^{VI}R$ isolines in the lower part of the diagram.

### *Trioctahedral and dioctahedral mica end-members*

It follows from the preceding discussion that the composition of common K micas can be shown in a polygon outlined by seven ideal members (as vertices) (see Fig. 1, and more specifically, Fig. 7). Sequentially clockwise these ideal members are: phlogopite $Mg_3$ (3;0), $Mg_{2.5}Al_{0.5}$ ['aluminian phlogopite'] (2.5;−0.5), $Al_{2.167}\square_{0.833}$ ['trans-muscovite'] (0;−2.167), $Al_{1.75}Li_{1.25}$ ['Fe-free zinnwaldite']

TABLE 1. Occupancy of octahedral and tetrahedral sites in some defined ideal common trioctahedral K micas, arranged according to *mgli* lines. The *mgli–feal* coordinates (in parantheses) accompany each mica name. tm: transitional mica.

| *mgli* | Ideal mica | Octahedral | | | | | | Tetrahedral | | | |
|---|---|---|---|---|---|---|---|---|---|---|---|
| | | Mg | Fe | $^{VI}$Al | Li | $^{VI}R$ | $^{VI}$ch | $^{IV}$Al | Si | $^{IV}$ch | Si/$^{IV}$Al |
| +3 | Phlogopite (3;0) | 3 | 0 | 0 | 0 | 3 | 6 | 1 | 3 | 15 | 3 |
| +2.5 | 'Ferroan phlogopite' (2.5;0.5) | 2.5 | 0.5 | 0 | 0 | 3 | 6 | 1 | 3 | 15 | 3 |
| +2.5 | Phlogopite (2.5;0) | 2.5 | 0.25 | 0.25 | 0 | 3 | 6.25 | 1.25 | 2.75 | 14.75 | 2.2 |
| +2.5 | 'Magnesian phlogopite' (2.5;−0.5) | 2.5 | 0 | 0.5 | 0 | 3 | 6.5 | 1.5 | 2.5 | 14.5 | 1.67 |
| +2 | 'Ferroan phlogopite' (2;1) | 2 | 1 | 0 | 0 | 3 | 6 | 1 | 3 | 15 | 3 |
| +2 | Phlogopite (2;0) | 2 | 0.375 | 0.375 | 0 | 2.75 | 5.875 | 0.875 | 3.125 | 15.125 | 3.57 |
| +2 | IMA eastonite (2;−1) | 2 | 0 | 1 | 0 | 3 | 7 | 2 | 2 | 14 | 1 |
| +1 | Biotite (1;2) | 1 | 2 | 0 | 0 | 3 | 6 | 1 | 3 | 15 | 3 |
| +1 | Biotite (1;1) | 1 | 1.5 | 0.5 | 0 | 3 | 6.5 | 1.5 | 2.5 | 14.5 | 1.67 |
| +1 | Tainiolite (1;0) | 2 | 0 | 0 | 1 | 3 | 5 | 0 | 4 | 16 | ∞ |
| 0 | Annite (0;3) | 0 | 3 | 0 | 0 | 3 | 6 | 1 | 3 | 15 | 3 |
| 0 | Annite (0;2) | 0 | 2.5 | 0.5 | 0 | 3 | 6.5 | 1.5 | 2.5 | 14.5 | 1.67 |
| 0 | Annite (0;2) | 0 | 2.375 | 0.375 | 0 | 2.75 | 5.875 | 0.875 | 3.125 | 15.125 | 3.57 |
| 0 | Siderophyllite (0;1) | 0.25 | 1.75 | 0.75 | 0.25 | 3 | 6.5 | 1.5 | 2.5 | 14.5 | 1.67 |
| 0 | Siderophyllite (0;1) | 0.125 | 1.75 | 0.75 | 0.125 | 2.75 | 6.125 | 1.125 | 2.875 | 14.875 | 2.56 |
| 0 | IMA siderophyllite (0;1) | 0 | 2 | 1 | 0 | 3 | 7 | 2 | 2 | 14 | 1 |
| 0 | Siderophyllite (0 0) (tm) | 0.25 | 1 | 1 | 0.25 | 2.5 | 5.75 | 0.75 | 3.25 | 15.25 | 4.33 |
| 0 | Siderophyllite (0;0) (tm) | 0 | 1.25 | 1.25 | 0 | 2.5 | 6.25 | 1.25 | 2.75 | 14.75 | 2.2 |
| 0 | Member $Al_3$ (0;−3) 'hyper-muscovite' | 0 | 0 | 3 | 0 | 3 | 4 | 0 | 12 | 0 | |
| −0.5 | Annite (−0.5;2.5) | 0 | 2.5 | 0 | 0.5 | 3 | 5.5 | 0.5 | 3.5 | 15.5 | 7 |
| −0.5 | Annite (−0.5;2) | 0 | 2.25 | 0.25 | 0.5 | 3 | 5.75 | 0.75 | 3.25 | 15.25 | 4.33 |
| −0.5 | Siderophyllite (−0.5;1) | 0 | 1.75 | 0.75 | 0.5 | 3 | 6.25 | 1.25 | 2.75 | 14.75 | 2.2 |
| −0.5 | Siderophyllite (−0.5;0.5) 'protolithionite' | 0 | 1.5 | 1 | 0.5 | 3 | 6.5 | 1.5 | 2.5 | 14.5 | 1.67 |
| −0.5 | Siderophyllite (−0.5;0) | 0 | 1.125 | 1.125 | 0.5 | 2.75 | 6.125 | 1.125 | 2.875 | 14.875 | 2.56 |
| −0.5 | Siderophyllite (−0.5;−0.5) (tm) | 0 | 0.75 | 1.25 | 0.5 | 2.5 | 5.75 | 0.75 | 3.25 | 15.25 | 4.33 |

| | | | | | | | | | | |
|---|---|---|---|---|---|---|---|---|---|---|
| −1 | 'Al-free zinnwaldite' (−1;2) | 0 | 2 | 0 | 1 | 3 | 5 | 0 | 4 | 16 | ∞ |
| −1 | Zinnwaldite (−1;0) | 0 | 1 | 1 | 1 | 3 | 6 | 1 | 3 | 15 | 3 |
| −1 | Zinnwaldite (−1;−1) (tm) | 0 | 0.25 | 1.25 | 1 | 2.5 | 5.25 | 0.25 | 3.75 | 15.75 | 15 |
| −1 | Zinnwaldite (−1;−1.83) | 0 | 0 | 1.83 | 1 | 2.83 | 6.5 | 1.5 | 2.5 | 14.5 | 1.67 |
| −1 | 'K-ephesite' (−1;−2) | 0 | 0 | 2 | 1 | 3 | 7 | 2 | 2 | 14 | 1 |
| −1.25 | 'Fe-free zinnwaldite' (−1.25;−1.75) | 0 | 0 | 1.75 | 1.25 | 3 | 6.5 | 1.5 | 2.5 | 14.5 | 1.67 |
| −1.5 | 'Ferroan trilithionite' (−1.5;0.5) | 0 | 1 | 0.5 | 1.5 | 3 | 5 | 0 | 4 | 16 | ∞ |
| −1.5 | Lepidolite (−1.5;0) | 0 | 0.75 | 0.75 | 1.5 | 3 | 5.25 | 0.25 | 3.75 | 15.75 | 15 |
| −1.5 | Lepidolite (−1.5;−0.5) 'cryophyllite' | 0 | 0.5 | 1 | 1.5 | 3 | 5.5 | 0.5 | 3.5 | 15.5 | 7 |
| −1.5 | Lepidolite (−1.5;−1.25) | 0 | 0.125 | 1.375 | 1.5 | 3 | 5.875 | 0.875 | 3.125 | 15.125 | 3.57 |
| −1.5 | Trilithionite (−1.5;−1.5) | 0 | 0 | 1.5 | 1.5 | 3 | 6 | 1 | 3 | 15 | 3 |
| −2 | Polylithionite (−2;−1) | 0 | 0 | 1 | 2 | 3 | 5 | 0 | 4 | 16 | ∞ |

(−1.25;−1.75), polylithionite $Li_2Al$ (−2;−1), $Fe^{2+}_2Li$ ['Al-free zinnwaldite'] (−1;2) and annite $Fe^{2+}_3$ (0;3). Theoretical IMA siderophyllite $Fe^{2+}_2Al$ and naturally occurring siderophyllite such as $Fe^{2+}_{1.75}Al_{0.75}Mg_{0.25}Li_{0.25}$ (both with 0;1) plot inside the polygon. Trilithionite $Al_{1.5}Li_{1.5}$ (−1.5;−1.5) and the compositional points $Li_{1.5}Fe^{2+}Al_{0.5}$ ['ferroan trilithionite'] (−1.5;0.5), $Fe^{2+}_2Mg$ ['biotite'] (1;2), and $Mg_2Fe^{2+}$ ['ferroan phlogopite'] (2;1) plot on the circumference of the polygon. The position of tainiolite $Mg_2Li$ (1;0) in the diagram is unique, reflecting its isolated status within the K-mica system. The polygon encloses all conceivable trioctahedral and dioctahedral K-mica species involving 22 charges.

The common true dioctahedral K micas form another, smaller polygon within the one described above, which is also outlined by seven compositional points (see Fig. 1, and more specifically Fig. 8): celadonite $Fe^{3+}Mg\square$ (1;1) (plotting in the trioctahedral portion of the polygon, see below), $Al_{1.5}Mg\square_{0.5}$ ['magnesian muscovite'] (1;−1,5), $Al_{2.17}\square_{0.83}$ ['trans-muscovite'] (0;−2.17), $Al_{1.83}Li\square_{0.17}$ ['lithian muscovite'] (−1;−1.83), $Al_{1.25}LiFe^{2+}_{0.25}\square_{0.5}$ ['lithian phengite'] (−1;−1), ferro-aluminoceladonite $AlFe^{2+}\square$ (0;0), and ferroceladonite $Fe^{3+}Fe^{2+}\square$ (0;2) (the last one also plots in the trioctahedral portion of the polygon). Muscovite $Al_2\square$ (0;−2) is positioned inside that polygon and is the most Al-rich mica with the smallest octahedral occupancy ($^{VI}R = 2$).

Celadonites are dioctahedral micas the tetrahedral sheet of which is mostly occupied by Si cations. Four end-members forming solid solutions are distinguished (e.g. Li *et al*., 1997; Rieder *et al*., 1998). As seen in Fig. 1, celadonite (1;1), aluminoceladonite (1;−1), ferro-aluminoceladonite (0;0), and ferroceladonite (0;2) plot as a parallelogram within the polygon. Celadonites do not contain any substantial Li, but most of them bear $Fe^{3+}$ forming an essential constituent in the formula (see Hendricks and Ross, 1941; Wise and Eugster, 1964; Foster, 1967, 1969; Buckley *et al*., 1978). Because of the presence of $Fe^{3+}$ in the formula, celadonitic micas require a special comment when plotting in terms of *mgli* and *feal*. $Fe^{3+}$-free celadonites representing the bottom members in the celadonite parallelogram, i.e. (0;0), (0.5;−0.5) and (1;−1), fall in an area that is not occupied by common trioctahedral K micas. A special situation arises with Fe-richer ($Fe^{3+}$-bearing) celadonites, which overlap with both common trioctahedral K micas and tainiolite. To avoid this complication, celadonites must be

TABLE 2. Occupancy of octahedral and tetrahedral sites in some defined ideal common dioctahedral K micas, arranged according to *mgli* lines. The *mgli-feal* coordinates (in parantheses) accompany each mica name. tm: transitional mica.

| *mgli* | Ideal mica | Octahedral | | | | | | | Tetrahedral | | | |
|---|---|---|---|---|---|---|---|---|---|---|---|---|
| | | Mg | $Fe^{2+}$ | $Fe^{3+}$ | $^{VI}Al$ | Li | $^{VI}R$ | $^{VI}ch$ | $^{IV}Al$ | Si | $^{IV}ch$ | $Si/^{IV}Al$ |
| +1 | Celadonite (1;1) | 1 | 0 | 1 | 0 | 0 | 2 | 5 | 0 | 4 | 16 | ∞ |
| +1 | Celadonite/aluminium celadonite (1;0) | 1 | 0 | 0.5 | 0.5 | 0 | 2 | 5 | 0 | 4 | 16 | ∞ |
| +1 | Aluminoceladonite (1;−1) | 1 | 0 | 0 | 1 | 0 | 2 | 5 | 0 | 4 | 16 | ∞ |
| +1 | 'Magnesian muscovite' (1;−1.5) (tm) | 1 | 0 | | 1.5 | 0 | 2.5 | 6.5 | 1.5 | 2.5 | 14.5 | 1.67 |
| +0.5 | 'Ferriceladonite' (0.5,1.5) | 0.5 | 0 | 1.5 | 0 | 0 | 2 | 5.5 | 0.5 | 3.5 | 15.5 | 7 |
| +0.5 | Ferroceladonite/celadonite (0.5;1.5) | 0.5 | 0.25 | 1.25 | 0 | 0 | 2 | 5.2 | 0.25 | 3.75 | 15.75 | 15 |
| +0.5 | Ferroceladonite/celadonite (0.5;1.5) | 0.5 | 0.5 | 1 | 0 | 0 | 2 | 5 | 0 | 4 | 16 | ∞ |
| +0.5 | Fe cel/cel/Fe-Al cel/Al cel (0.5;0.5) | 0.5 | 0.5 | 0.5 | 0.5 | 0 | 2 | 5 | 0 | 4 | 16 | ∞ |
| +0.5 | Ferro-aluminoceladonite/aluminoceladonite (0.5;−0.5) | 0.5 | 0.5 | 0 | 1 | 0 | 2 | 5 | 0 | 4 | 16 | ∞ |
| +0.5 | Phengite (0.5;−1) | 0.5 | 0.25 | | 1.25 | 0 | 2 | 5.25 | 0.25 | 3.75 | 15.75 | 15 |
| +0.5 | Muscovite (0.5;−1.5) | 0.5 | 0 | | 1.5 | 0 | 2 | 5.5 | 0.5 | 3.5 | 15.5 | 7 |
| +0.33 | Phengite (0.33;−1) | 0.33 | 0.33 | | 1.34 | 0 | 2 | 5.34 | 0.34 | 3.66 | 15.66 | 10.765 |
| 0 | 'Ferri muscovite' (0;2) | 0 | 0 | 2 | 0 | 0 | 2 | 6 | 1 | 3 | 15 | 3 |
| 0 | Ferroceladonite (0;2) | 0 | 1 | 1 | 0 | 0 | 2 | 5 | 0 | 4 | 16 | ∞ |
| 0 | Ferroceladonite/ferro-aluminoceladonite (0;1) | 0 | 1 | 0.5 | 0.5 | 0 | 2 | 5 | 0 | 4 | 16 | ∞ |
| 0 | Ferro-aluminoceladonite (0;0) | 0 | 1 | 0 | 1 | 0 | 2 | 5 | 0 | 4 | 16 | ∞ |
| 0 | Phengite (0;−1) | 0 | 0.5 | | 1.5 | 0 | 2 | 5.5 | 0.5 | 3.5 | 15.5 | 7 |
| 0 | Muscovite (0;−2) | 0 | 0 | | 2 | 0 | 2 | 6 | 1 | 3 | 15 | 3 |
| 0 | Member $Al_{2.167}$ (0;−2.167) 'trans-muscovite' | 0 | 0 | | 2.167 | 0 | 2.17 | 6.5 | 1.5 | 2.5 | 14.5 | 1.67 |
| 0 | Member $Al_{2.5}$ (0;−2.5) (tm) 'hyper-muscovite' | 0 | 0 | | 2.5 | 0 | 2.5 | 7.5 | 2.5 | 1.5 | 13.5 | 0.6 |
| −0.5 | Phengite (−0.5;−1) (tm) | 0 | 0.5 | | 1.5 | 0.5 | 2.5 | 6 | 1 | 3 | 15 | 3 |
| −0.5 | Phengite (−0.5;−1) | 0 | 0.375 | | 1.375 | 0.5 | 2.25 | 5.375 | 0.375 | 3.625 | 15.625 | 9.67 |
| −0.5 | Muscovite (−0.5;−1.5) | 0 | 0.125 | | 1.625 | 0.5 | 2.25 | 5.625 | 0.625 | 3.375 | 15.375 | 5.4 |
| −0.5 | Muscovite (−0.5;−1.5) | 0 | 0 | | 1.5 | 0.5 | 2 | 5 | 0 | 4 | 16 | ∞ |
| −0.5 | Muscovite (−0.5;−2) | 0 | 0 | | 1.75 | 0.5 | 2.25 | 5.75 | 0.75 | 3.25 | 15.25 | 4.33 |
| −0.5 | Muscovite (−0.5;−2) (tm) | 0 | 0 | | 2 | 0.5 | 2.5 | 6.5 | 1.5 | 2.5 | 14.5 | 1.67 |
| −1 | 'Lithian phengite' (−1;−1) (tm) | 0 | 0.25 | | 1.25 | 1 | 2.5 | 5.25 | 0.25 | 3.75 | 15.75 | 15 |
| −1 | 'Lithian muscovite' (−1;−1.5) (tm) | 0 | 0 | | 1.5 | 1 | 2.5 | 5.5 | 0.5 | 3.5 | 15.5 | 7 |
| −1 | 'Lithian muscovite' (−1;−1.83) | 0 | 0 | | 1.83 | 1 | 2.83 | 6.5 | 1.5 | 2.5 | 14.5 | 1.67 |

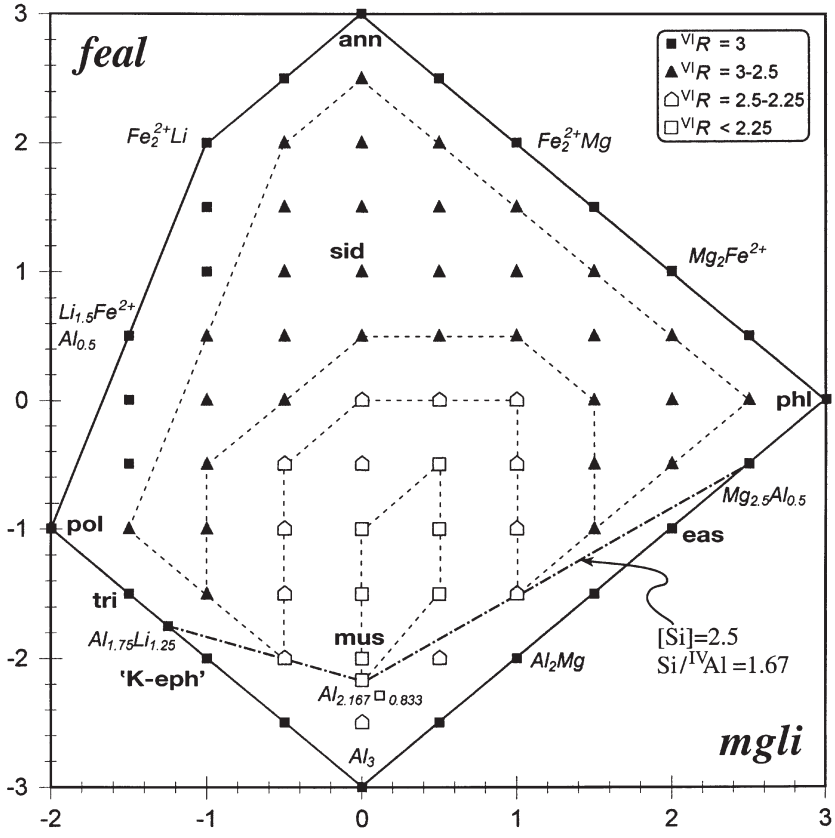


FIG. 3. Ideal octahedral occupancy for common K micas ($^{VI}R$) corresponding to $XY_{2-3}Z_4O_{10}(OH,F)_2$ (excluding tainiolite and $Fe^{3+}$-bearing celadonites) plotted on the *mgli–feal* grid. $^{VI}R$ areas, and one [Si] isoline, which divides the area with [Si] >2.5 (above) from that with [Si] <2.5 (below) are shown. The only exception is the IMA siderophyllite with [Si] = 2 for *mgli* = 0 and *feal* = 1. Abbreviations as in Fig. 1.

plotted separately from trioctahedral micas in the polygon (see discussion of Fig. 8 below). As seen by comparing the two vertical boundaries of the celadonite parallelogram, for celadonites with *mgli* = 1, and 0, the content of divalent Fe is constant 0, and 1 (a.p.f.u.), respectively. In all situations, the amount of trivalent Fe increases with increasing *feal*, from 0 up to 1 (a.p.f.u.) (see also Table 2).

### *Distribution of natural micas in the diagram*

When examining published data, no systematic preferences or avoidances were used. Hence, the relative frequencies of points in the plots represent what hopefully is a random sample drawn of the totality of published mica compositions. Moreover, care was taken to ascertain that they correspond to a single mica rather than a mixture of several phases.

In Fig. 4, trioctahedral mica compositions ($n$ = 2381) taken from previous compilations by Tischendorf *et al*. (1997, 1999, 2001*a*,*b*) and from Brigatti and Guggenheim (2002, their Table 1, and their Table 2 for dioctahedral micas) are plotted in terms of *mgli vs*. *feal*. The distribution of the points within the polygon is non-uniform, with density in the marginal portions higher than that in the central portion. This distribution pattern applies especially to the Mg-Fe mica sector, whereas the occupancy of the Li-Fe and Li-Al sectors is more balanced. The area adjacent to zinnwaldite (−1;0) is occupied by numerous mica compositions. In contrast, the Li-Fe and the Mg-Al sectors contain remarkably few data. The part of the diagram to

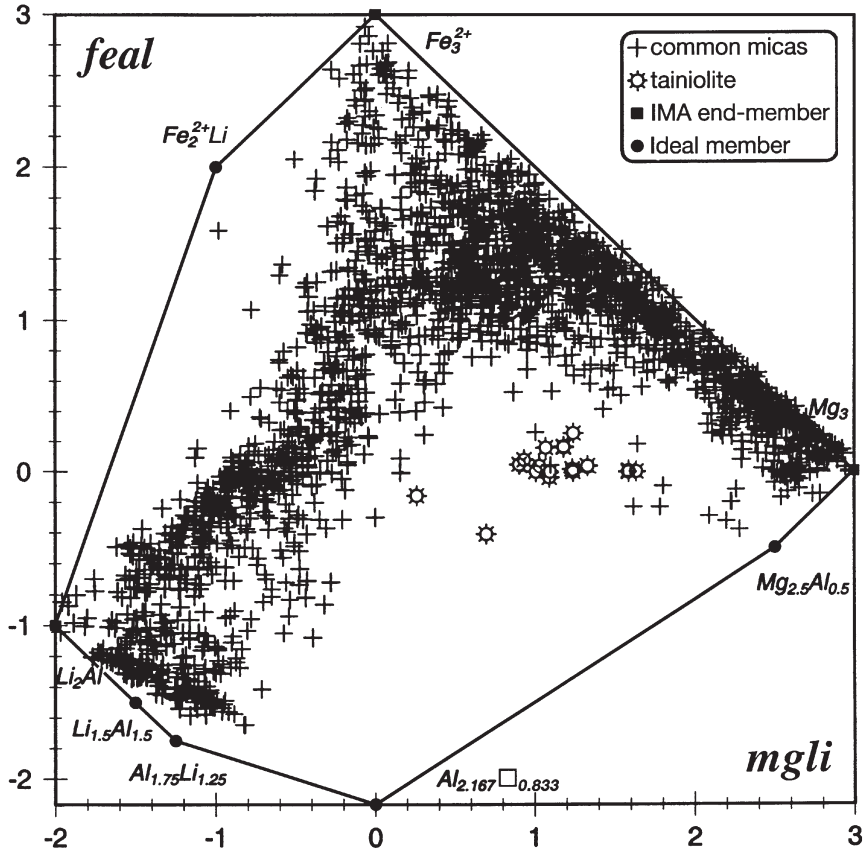


FIG. 4. Distribution of common trioctahedral K micas (+ $n$ = 2362) and tainiolites (☼, $n$ = 19) in the *mgli–feal* diagram.

the right of the centre contains only very few common trioctahedral micas and is occupied by tainiolite alone.

Muscovitic and phengitic micas (see Fig. 5; $n$ = 1046) are concentrated in the diagram close to *mgli* = 0 and *feal* = −1.5. Fe-bearing phengites are spread out (a result of much of their Fe being trivalent), but Mg-bearing phengites (Mg >0.5 a.p.f.u.) are rare, reflecting the long recognized special metamorphic conditions (high pressure) required for their formation.

Celadonites ($n$ = 95) plot in an area defined by *mgli* from 0 to 1, and *feal* from 2 to −1. Natural celadonitic micas exist that plot close to *mgli* = 0.5 and *feal* = 1.5 (the divide between ferroceladonite and celadonite) and contain 0.5 Mg, <0.5 $Fe^{2+}$, and up to 1.5 $Fe^{3+}$. It might be justified to accept another celadonite end-member with a formula K $Fe^{3+}_{1.5}Mg_{0.5}\square Al_{0.5}Si_{3.5}O_{10}(OH)_2$ ['ferriceladonite'] at (0.5;1.5). The density of points clustering around *mgli* = 0.5; *feal* = 1.5 supports this suggestion. Celadonites of this composition were described by Adamson and Richards (1990) and Teagle *et al*. (1996).

## Discussion and mica subdivision using *mgli* and *feal*

### *Mica frequency in the diagram*

The density of points in the *mgli–feal* diagram is irregular. The bulk of the data is consistent with the well-known four major mica series in nature, which overlap each other (see Figs 4, 5, 7, 8):

(a) phlogopite (3;0) – biotite (1;2) – annite (0;3); vector: $Mg[Fe^{2+}]_{-1}$,

(b) biotite (1;2) – siderophyllite (0;1) – zinnwaldite (−1;0) – lepidolite (−2;−1); vector: $2Fe^{2+}Mg^{IV}Al[2Li^{VI}AlSi]_{-1}$,

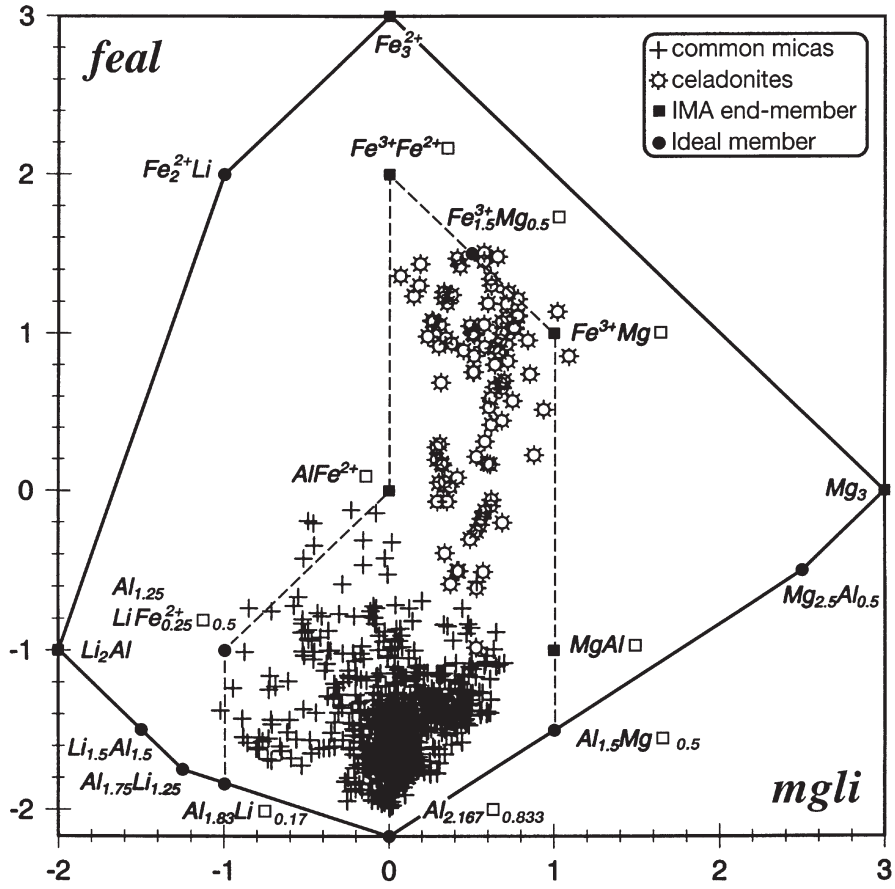


FIG. 5. Distribution of common dioctahedral K micas (+, $n$ = 1046) and celadonites (☼, $n$ = 95) in the *mgli–feal* diagram.

(c) lepidolite (−2;−1) – zinnwaldite (−1;−1.5) – muscovite (0;−2); vector: $^{VI}Al^{IV}Al[2LiSi]_{-1}$, and

(d) muscovite (0;−2) – phengite (0.33;−1) – celadonite (1;1); vector: $2^{VI}Al^{IV}Al[Fe^{3+}MgSi]_{-1}$.

With the exception of micas of the phlogopite–annite solid-solution series, mica compositions that plot along the borders of the polygon correspond to extreme compositions that in nature will occur only rarely. This is in contrast to overpopulated areas (muscovite/Mg-rich siderophyllite/zinnwaldite), inside the polygon are areas with very few compositions or none at all. Such poorly populated areas especially concern the sector *mgli* >0.5; *feal* <−0.5, but also marginal parts of the Li-Fe mica group. The reason for the heterogeneity in population of the diagram is poorly understood, but is unlikely to be an artefact of collection of literature data. Instead, petrological controls, miscibility gaps or other reasons associated with the crystal structure may have prevented some compositions from growing as an homogeneous phase.

### *Transitional micas*

Plotting micas in the *mgli–feal* diagram permits checking their real *vs*. predicted octahedral occupancy and evaluating their proximity to maxima ($^{VI}R \approx 3$) or minima ($^{VI}R \approx 2$). The conventional divide between trioctahedral and dioctahedral micas lies at $^{VI}R = 2.5$. An isozone for $^{VI}R \approx 2.5$ (based on idealized formulas) is recognizable in Fig. 3. However, because the

correlation between the numerical value of $^{VI}R$ and *mgli* or *feal* is not particularly rigorous, in determining the tri- or dioctahedral character of a mica, one should always give priority to the calculated mica formula, not to the position of the mica in the diagram.

### *The position of Li-rich micas in the diagram*

In the *mgli–feal* diagram, the uncommon mica tainiolite, ideal formula $KMg_2LiSi_4O_{10}F_2$ – (1;0), plots in an area (*mgli* = 0.75 to 1.5; *feal* = −0.25 to 0.25), where micas with three octahedral cations are not to be expected, but instead where Li-free dioctahedral micas resembling $Fe^{2+}$-free celadonites are positioned. By virtue of the definition of *mgli* and *feal*, compositions like $KMgFe^{2+}_{0.625}Al_{0.625}\square_{0.75}Al_{0.125}Si_{3.875}O_{10}(OH)_2$ or $KMgFe^{2+}_{0.75}Al_{0.75}\square_{0.5}Al_{0.125}Si_{3.875}O_{10}(OH)_2$ coincide with theoretical tainiolite, but fortunately do not form in nature.

Tainiolite and polylithionite are trioctahedral mica end-members, which contain maximum enrichment of Li and are represented by two points far apart in the *mgli–feal* diagram. Natural tainiolite contains minimal amounts of Fe and Al only; polylithionite (or, strictly speaking, the variety lepidolite) is practically Fe-free and either Al-rich or Al-poor. Micas with elevated Li and Mg contents, and at the same time lowered Fe and Al contents, plot between those points in the *mgli–feal* diagram, thus forming a 'bridge'. Micas enriched in both Mg and Li are known to form in association with alkaline to peralkaline rocks (Hawthorne *et al*., 1999; Pesquera *et al*., 1999) in a Li-Mg-enriched environment of crystallization (see Tischendorf *et al*., 1999, their Table 6). In contrast to tainiolite and polylithionite, several of these micas have low $Si/^{IV}Al$ ratios (~2 to 4) and some of them, especially those of Lapides *et al*. (1977), are dioctahedral and can formally be assigned to Li-bearing phengite. The incompletely described "magnesium zinnwaldite" of Semenov and Shmakin (1988) may belong to these micas. To define this species as an intermediate member on the tieline tainiolite–polylithionite, its formula should be $KLi_{0.78}Mg_{0.78}Al_{0.66}Fe^{2+}_{0.33}\square_{0.44}Si_4O_{10}(OH,F)_2$ (0; −0.33) instead of $KLiMgAlAlSi_3O_{10}(OH,F)_2$ (0;−1) which better fulfills the conditions of a constituent of that tieline. Anyway, the currently available data do not suffice for a qualified decision about the status of "magnesium zinnwaldite".

### *Mica stability as function of [Si]*

Our extensive mica database did not contain even a single mica, the [Si] content of which is <2.5; a value that apparently exerts some compelling control over the stability of natural K micas. Theoretically, K micas possessing [Si] contents between 2.5 and 2.0, the lower stability limit of micas according to Loewenstein's (1954) rule, could form, but apparently do not exist in nature. This observation implies that compositions corresponding to IMA-accepted K-mica formulas with [Si] = 2 such as siderophyllite $[KFe^{2+}_2Al Al_2Si_2O_{10}(OH)_2]$ and eastonite $[KMg_2AlAl_2Si_2 O_{10}(OH)_2]$ represent hypothetical, ideal end-members only, but are not to be expected to exist in nature. Indeed, type eastonite from Easton, Pennsylvania, has been shown later not to be an homogenous phase but a mixture of phlogopite and serpentine (Livi and Veblen, 1987).

Although IMA-siderophyllite (0;1) with [Si] = 2 has been synthesized (Rieder, 1971), this mica also represents a theoretical species only. In natural siderophyllite (n >600), octahedrally coordinated Fe and Al are usually substituted by small quantities of Mg and Li. These substitutions alter the composition in a way such that natural siderophyllite takes [Si] $\geqslant$2.5. Substitution of 0.125 or 0.25 a.p.f.u. Mg and Li, which would match the composition of average natural siderophyllite more closely, would result in more realistic formulas for siderophyllite (0;1), namely $KFe^{2+}_{1.75}Al_{0.75}Mg_{0.125}Li_{0.125}\square_{0.25}Al_{1.125}Si_{2.875}O_{10}(OH)_2$ or, even better, $KFe^{2+}_{1.75}Al_{0.75}Mg_{0.25}Li_{0.25}Al_{1.5}Si_{2.5}O_{10}(OH)_2$. The presence of all four essential octahedrally coordinated cations in siderophyllite is apparently more appropriate for its central location in the diagram (and the whole mica group).

With respect to [Si], K micas apparently behave differently from Na micas. In natural, K-free ephesite $[Na Al_2Li Al_2Si_2 O_{10}(OH)_2]$, the contents of [Si] range from 2.01 (Schaller *et al*., 1967) to 2.20 (Semenov, 2001). However, the K-analogue of ephesite, which is included in the vector system of Černý and Burt (1984) and Burt (1991), and which would have a theoretical composition at (−1;−2) in our diagram (see Fig. 1), is not yet known as a stable natural compound. Apparently, the Na micas with their larger tetrahedral rotation (e.g. compare paragonite *vs.* muscovite; Bailey, 1984) better allow the Loewenstein limit to be approached.

### *Al-free zinnwaldite*

To complement the system of common K micas, it might be useful to introduce yet another mica end-member, namely 'Al-free zinnwaldite', $KFe^{2+}_2LiSi_4O_{10}F_2$ (−1;2), ideal composition (in wt.%) 49.7 $SiO_2$, 29.7 FeO, 3.1 $Li_2O$, 9.7 $K_2O$, and 7.8 F. This mica is not listed by the IMA mica subcommittee, but is integrated in the vector system of Černý and Burt (1984) and Burt (1991). Micas resembling 'Al-free zinnwaldite' are reported from the Pikes Peak batholith (Kile and Foord, 1998; Brigatti *et al*., 2000) and from pegmatites of Minagi, Japan (Ukai *et al*., 1956, their sample 3).

### *The muscovite–celadonite series*

Rieder *et al*. (1998, their Fig. 1*a*) imply a continuous miscibility between the end-members muscovite and aluminoceladonite. Massonne and Schreyer (1986) described the existence of extensive miscibility in this series offering a substitution equation $^{VI}(Mg,Fe^{2+}) + {}^{[VI]}(Fe^{3+}) + {}^{[IV]}Si \rightarrow {}^{[VI]}Al + {}^{[IV]}Al$, which includes all celadonitic micas.

If we limit our discussion of this series to the variables ($Fe_{tot}$ + Mg) and Si, a fairly strong positive correlation between both parameters is observed for muscovite, phengite, aluminoceladonite, and ferroan-aluminian celadonite along the line from (Si = 3; Mg + $Fe_{tot}$ = 0) to (Si = 4; Mg + $Fe_{tot}$ = 1) (Fig. 6). Deviations from this line can be attributed to either the presence of $Fe^{3+}$ (determined or not) or, to a limited extent, to high Mg contents such as exist in micas of the Mg-Li group. A significant proportion of $Fe_{tot}$ in muscovite must be present as $Fe^{3+}$, inasmuch as the charge of the octahedral sheet is controlled by $^{IV}Si$. The high proportion of $Fe^{3+}$ in celadonite must have brought about a reduction of Si from 4 to 3.5 (a.p.f.u.), which apparently is decisive for the formation of ferriceladonite. The fact that most of the Fe in natural dioctahedral K micas may be $Fe^{3+}$ is consistent with the results of Guidotti *et al.* (1994), who showed that even in reduced, graphite-bearing schists, >50% of total Fe in white mica is trivalent (see also Guidotti and Sassi, 1998). The Mg content of muscovite/phengite is limited. In muscovite from highly metamorphosed rocks it reaches 0.7 a.p.f.u., whereas experimentally prepared muscovite may contain up to 1.0 Mg a.p.f.u. (see Schmidt *et al*., 2001).

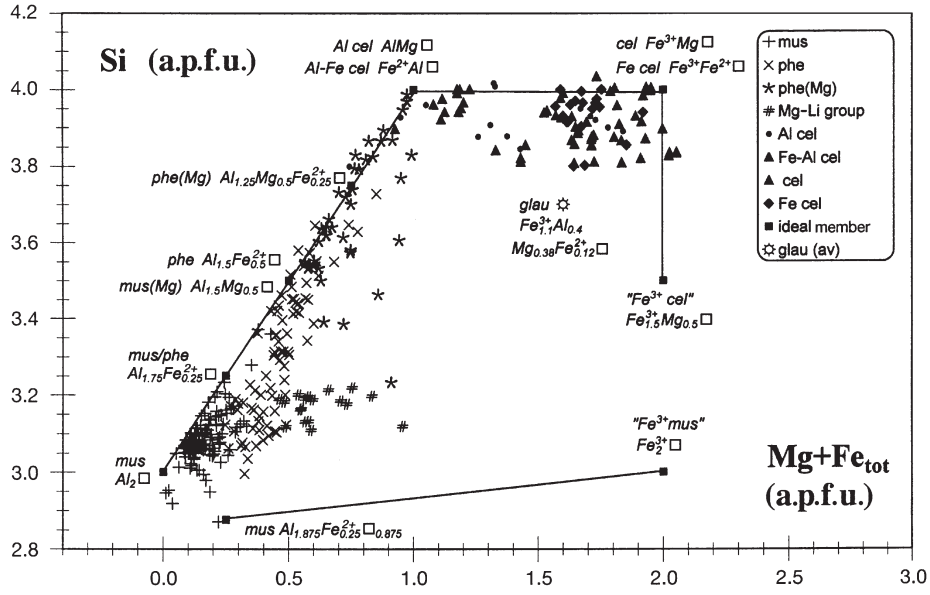


FIG. 6. Correlation between Si (a.p.f.u.) and Mg+$Fe_{tot}$ (a.p.f.u.) for muscovites, phengites and celadonite varieties. The numbers of muscovite and phengite analyses are statistically reduced. Lines $x = 0$; $y = 3$ to $x = 1$; $y = 4$ as well as $x = 1$ to $x = 2$ at $y = 4$ correspond to micas with $^{VI}R = 2.0$. The mean composition of glauconite ($n = 98$) is shown for comparison. For abbreviations see Fig. 1.

### *Mica names and boundaries for subdivision*

The subdivision of common true K micas proposed in this paper closely follows the general principles of mineral classification formulated by the IMA (Nickel and Grice, 1998) and only uses mineral names approved as end-member or series names in the current mica nomenclature elaborated by Rieder *et al*. (1998). The fields of the mica varieties discriminated in the polygon have borders, which usually are parallel to the *feal* or *mgli* axes (Table 3, Figs 7,8). These borderlines are best suited to handling and classifying all the mica series, which plot in the diagram as oblique lines of variable slope. The selection of borderlines in terms of *mgli* and *feal* also embodied historical aspects of the quantitative discrimination between the varieties as already used in Foster (1960*a*,*b*). Accordingly, names 'polylithionite' and 'trilithionite' refer to end-member and ideal-member names only, but are not assigned to fields defining mica varieties.

The discrimination between trioctahedral and dioctahedral micas requires consideration of octahedral occupancy (see Fig. 3). Boundaries of the celadonitic micas take advantage of their respective $^{VI}$Al, $Fe^{2+}$, $Fe^{3+}$ and Mg contents, respectively.

### *Petrological considerations*

Every K-mica variety forms in favourable environments. Members of the phlogopite–biotite–annite series dominate in mantle and lower-crust derived magmatic rocks, particularly in M-, I- and A-type granitoids. They also dominate among the common metamorphic rocks. The biotite–siderophyllite–zinnwaldite–lepidolite series occurs in upper-crustal magmatites, particularly in S-type granites and their derivatives (i.e. aplites, pegmatites, greisens). Concerning the distribution of micas in the Al-Li field, there are points that might correspond to transitional lepidolite-zinnwaldite-muscovite micas in the sense of Monier and Robert (1986). In this series, Li-Fe bearing muscovite occurs, which preferentially formed during late-magmatic recrystallization processes of evolved granites. Tainiolitic micas formed under unusual conditions, if Li-rich solutions meet Mg-rich country rocks. The muscovite–phengite series typifies metamorphic environments. Celadonitic micas are entirely confined to low-temperature processes. Micas of the join muscovite–phlogopite (or even directed to IMA eastonite) should not occur in nature. Magnesium incorporation in muscovite is limited and pressure dependent.

## Conclusions

Any mineral system with six or more variables demands simplification to make it suitable for visual inspection. The main advantage of the coordinates *mgli* and *feal* used in this paper as parameters for subdivision of common K micas is the herewith-achieved substantial reduction of required chemical variables to a system with only

TABLE 3. Compositional range of common K-mica varieties based on 22 cationic valences with respect to *mgli* and *feal* (see Figs 7 and 8).

| Mica variety | *mgli* | *feal* |
|---|---|---|
| Trioctahedral micas ($^{VI}R$ = 2.5 to 3) | | |
| Phlogopite | +2 ... +3 | (−1/0 ... +1/0) |
| Biotite | +1 ... +2 | (−1 ... +1/+2) |
| Annite | (−1/0 ... +1/0) | +2 ... +3 |
| Siderophyllite | −1 ... +1 | (−1/0 ... +2) |
| Zinnwaldite | −1.5 ... −1 | (−1.83/−1.5 ... +0.5/+2) |
| Lepidolite | −2 ... −1.5 | (−1.5/−1 ... −1/+0.5) |
| Tainiolite | ~+0.75 ... +1.5 | ~−0.25 ... +0.25 |
| Dioctahedral micas ($^{VI}R$ = 2 to 2.5) | | |
| Muscovite | (−1/0 ... +1/0) | −2.167 ... −1.5 |
| Phengite | (−1/0 ... +1/0) | −1.5 ... −1/0 |
| Celadonite | (0 ... +1) | −1/0 ... +1/+2 |

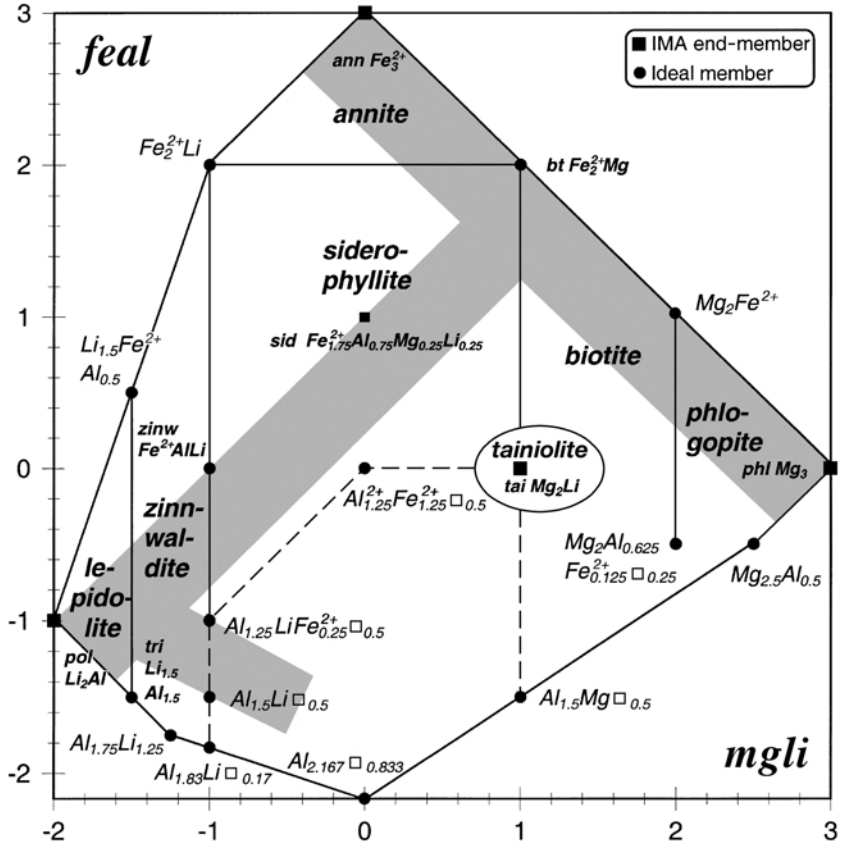


FIG. 7. Subdivision of common trioctahedral K-mica varieties in the *mgli–feal* diagram. The names of natural mica varieties are printed in italics. Shaded areas indicate solid-solution series. The broken line marks the boundary between trioctahedral and dioctahedral micas. Abbreviations and explanations as in Fig. 1.

two that can be presented in a simple and easy to handle, two-dimensional polygon. The limits of the polygon are defined by the octahedral occupancy, the condition of $22^+$-charges per formula, and by the observation that [Si] in natural K micas does not drop below 2.5.

The subdivision scheme proposed in this paper has several merits relative to previous approaches. By reduction to two parameters, the K-mica system is substantially simplified but not distorted. Only total Fe is required to calculate *feal*, which makes this system ideal for the classification of micas for which Fe valences have not been differentiated, i.e. chiefly for formulae based on microprobe analyses. The plot allows us to show Li-bearing micas alongside Li-free micas, and trioctahedral micas together with dioctahedral micas. Trioctahedral/dioctahedral (transitional) micas can be recognized by their position in the diagram. Moreover, it is advantageous to represent micas in the *mgli–feal* diagram using absolute values (a.p.f.u.) rather than relative values (percent or ratios). No calculation other than that of the mica formula is required.

The subdivision of K micas into varieties is accomplished by definition of fields in terms of the *mgli and feal* variables. The variation of *mgli* is powerful for classification purposes, because of the extended variability of the Mg/Li ratio from phlogopite to lepidolite. Subdivision along the *feal* axis is instrumental in deciding on the 'annitic' or 'muscovitic' character of the mica.

Mica compositions plotting outside of the polygons probably indicate an analytical artifact or an error in formula calculation. Thus, this proposed scheme permits recognition of some erroneous mica compositions and formulae.

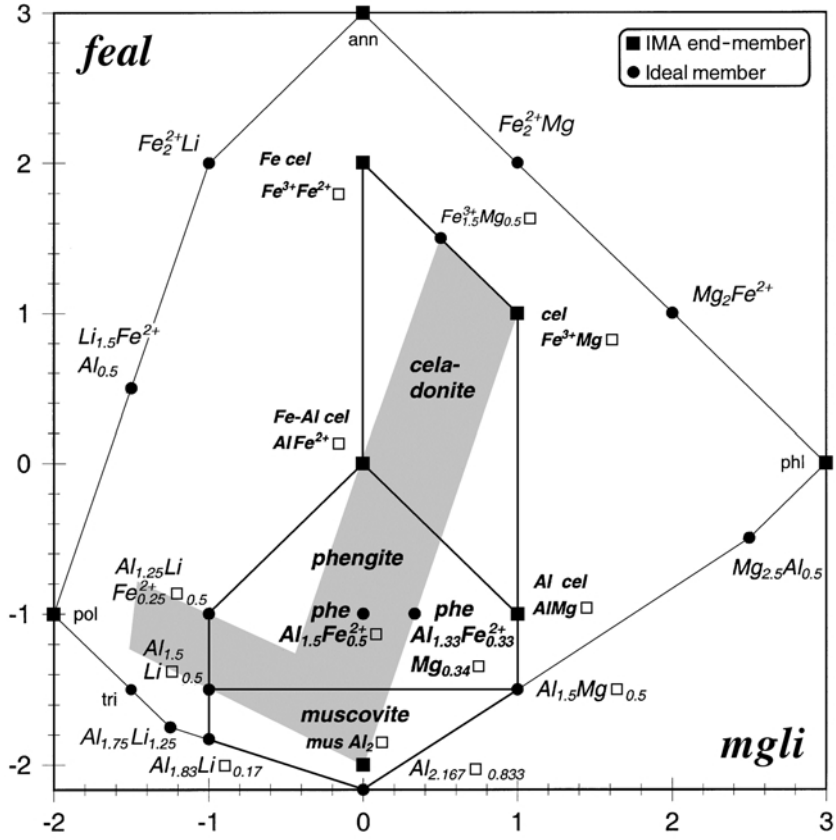


FIG. 8. Subdivision of common dioctahedral K-mica varieties in the *mgli–feal* diagram. The names of natural mica varieties are printed in italics. Shaded areas indicate solid-solution series. Abbreviations and explanations as in Fig. 1.

All K micas except of tainiolite and the group of celadonites are uniquely represented by the variables *mgli* and *feal*. Because of their unusual compositions (tainiolite: rich in Li and Mg; celadonites: poor in Li, but rich in $Fe^{3+}$) and conditions of formation, these micas can be recognized at an early stage of examination. If celadonitic micas are absent, tri- and dioctahedral K micas can certainly be treated together in the diagram.

Although several formulae can be calculated for one given point in the *mgli-feal* diagram because of balancing the charges of the tetrahedral and octahedral sheet (see Tables 1 and 2), the chemical composition of any mica is represented by one point only. Because the coordinates *mgli* (interval +3 to −2) and *feal* (interval +3 to −2.167) unambiguously characterize the composition of every common K mica except of the celadonites, they are superior to the 'Mg#' value. This value is defined merely as Mg/(Mg + $Fe_{tot}$) and constitutes a parameter widely used for the chemical characterization of micas. A much better description of mica composition would be achieved if the numerical values of *mgli* and *feal* are supplemented (in parentheses) to the variety name, or the term 'K mica' in general. For example, siderophyllite ($x = 0.00$; $y = 1.00$) or K mica (0;1) represents a sufficiently exact description of a mica variety occupying the central point of the whole Mg-Fe-Li-Al K-mica system.

In addition to the partial overlap of celadonitic micas with common trioctahedral K-mica compositions, our approach has the shortcoming that the vertical and horizontal boundaries are oblique to the major compositional trends of natural K micas. Acceptance of this minor disadvantage is

required in order to formulate a single classification that includes all common tri- and dioctahedral K micas.

## Acknowledgements

We would like to acknowledge Barrie Clarke, Halifax, for his detailed and constructive review. We wish to thank all colleagues who let us use their mica analyses or drew our attention to literature references, namely Bernard Bonin, Christian Chopin, both Paris, and Eric Essene, Ann Arbor. Bruce Velde, Paris, and Donald Burt, Tempe, are acknowledged for commenting on an earlier version of this paper.

## References

Adamson, A.C. and Richards, H.G. (1990) Low-temperature alteration of very young basalts from ODP Hole 648B: Serocki volcano, Mid-Atlantic Ridge. *Proceedings of the Ocean Drilling Program, scientific results*, **106/109**, (R.S. Detrick, J. Honnorez, W.B. Bryan., T. Juteau *et al*., editors), pp. 181–194.

Bailey, S.W. (1984) Crystal chemistry of the true micas. Pp. 13–60 in: *Micas* (S.W. Bailey, editor). Reviews in Mineralogy, **13**, Mineralogical Society of America, Washington, D.C.

Bragg, W.L. (1937) *Atomic Structure of Minerals*, 1st edition. Cornell University Press, USA, 292 pp.

Brigatti, M.F. and Guggenheim, S. (2002) Mica crystal chemistry and the influence of pressure, temperature, and solid solution on atomistic models. Pp. 1–97 in: *Micas: Crystal Chemistry and Metamorphic Petrology* (A. Mottana, F.P. Sassi, J.B. Thompson Jr. and S. Guggenheim, editors). Reviews in Mineralogy and Geochemistry, **46**, Mineralogical Society of America and the Geochemical Society, Washington, D.C.

Brigatti, M.F., Lugli, C., Poppi, L., Foord, E.E. and Kile, D.E. (2000) Crystal chemical variations in Li- and Fe-rich micas from Pikes Peak batholith (central Colorado). *American Mineralogist*, **85**, 1275–1286.

Buckley, H.A., Bevan, J.C., Brown, K.M., Johnson, L.R. and Farmer, V.C. (1978) Glauconite and celadonite: two separate mineral species. *Mineralogical Magazine*, **42**, 373–382.

Burt, D.M. (1991) Vector representation of lithium and other mica compositions. Pp. 113–129 in: *Progress in Metamorphic and Magmatic Petrology* (L.L. Perchuk, editor). Cambridge University Press, Cambridge, UK.

Černý, P. and Burt, D.M. (1984) Paragenesis, crystallochemical characteristics, and geochemical evolution of micas in granite pegmatites. Pp. 257–297 in: *Micas* (S.W. Bailey, editor) Reviews in Mineralogy, **13**, Mineralogical Society of America, Washington, D.C.

Foster, M.D. (1960*a*) Interpretation of the composition of trioctahedral micas. *US Geological Survey Professional Paper*, **354-B**, 11–49.

Foster, M.D. (1960*b*) Interpretation of the composition of lithium micas. *US Geological Survey Professional Paper*, **354-E**, 115–147.

Foster, M.D. (1967) Tetrasilicic dioctahedral micas – celadonite from near Reno, Nevada. *U.S. Geological Survey Professional Paper*, **575-C**, 17–22.

Foster, M.D. (1969) Studies of celadonite and glauconite. *US Geological Survey Professional Paper*, **614-F**, 1–17.

Gottesmann, B. and Tischendorf, G. (1978) Klassifikation, Chemismus und Optik trioktaedrischer Glimmer. *Zeitschrift für Geologische Wissenschaften*, **6**, 681–708.

Guidotti, C.V. and Sassi, F.P. (1998) Petrogenetic significance of Na-K white mica mineralogy: Recent advances for metamorphic rocks. *European Journal of Mineralogy*, **10**, 815–854.

Guidotti, C.V., Yates, M.G., Dyar, M.D. and Taylor, M.A. (1994) Petrogenetic implications of $Fe^{3+}$ content of muscovite in pelitic schists. *American Mineralogist*, **79**, 793–795.

Hawthorne, F.C., Teertstra, D.K. and Černý, P. (1999) Crystal-structure refinement of a rubidian cesian phlogopite. *American Mineralogist*, **84**, 778–781.

Heinrich, E.W. (1946) Studies in the mica group; the biotite-phlogopite series. *American Journal of Science*, **244**, 836–848.

Hendricks, S.B. and Ross, C.S. (1941) Chemical composition and genesis of glauconite and celadonite. *American Mineralogist*, **26**, 683–708.

Kile, D.E. and Foord, E.E. (1998) Micas from the Pikes Peak Batholith and its cogenetic granitic pegmatites, Colorado: Optical properties, composition, and correlation with pegmatite evolution. *The Canadian Mineralogist*, **36**, 463–482.

Koval', P.V., Kovalenko, V.I., Kuz'min, M.I., Pisarskaya, V.A. and Yurchenko, S.A. (1972) Mineral associations, composition and nomenclature of micas from rare-metal albite-bearing granitoids. *Doklady Akademii Nauk SSSR*, **202**, 1174–1177 (in Russian).

Lapides, I.L., Kovalenko, V.I. and Koval', P.V. (1977) *The Micas of Rare-Metal Granitoids*. Nauka, Novosibirsk, Russia, 103 pp. (in Russian).

Li, G., Peacor, D.R., Coombs, D.S. and Kawachi, Y. (1997) Solid solution in the celadonite family: The new minerals ferroceladonite, $K_2Fe^{2+}{}_2Fe^{3+}{}_2Si_8O_{20}(OH)_4$, and ferroaluminoceladonite, $K_2Fe^{2+}{}_2Al_2Si_8O_{20}(OH)_4$. *American Mineralogist*, **82**, 503–511.

Livi, K.J.T. and Veblen, D.R. (1987) 'Eastonite' from Easton, Pennsylvania: A mixture of phlogopite and a new form of serpentine. *American Mineralogist*, **72**, 113–125.

Loewenstein, W. (1954) The distribution of aluminum in the tetrahedra of silicates and aluminates. *American Mineralogist*, **39**, 92–96.

Massonne, H.-J. and Schreyer, W. (1986) High-pressure syntheses and X-ray properties of white micas in the system $K_2O$-MgO-$Al_2O_3$-$SiO_2$-$H_2O$. *Neues Jahrbuch für Mineralogie Abhandlungen*, **153**, 177–215.

Monier, G. and Robert, J.-L. (1986) Evolution of the miscibility gap between muscovite and biotite solid solutions with increasing lithium content: an experimental study in the system $K_2O$-$Li_2O$-MgO-FeO-$Al_2O_3$-$SiO_2$-$H_2O$-HF at 600ºC, 2 kbar $P_{H_2O}$: comparison with natural lithium micas. *Mineralogical Magazine*, **50**, 641–651.

Nickel, E.H. and Grice, J.D. (1998) The IMA Commission on New Minerals and Mineral Names: Procedures and guidelines on mineral nomenclature, 1998. *The Canadian Mineralogist*, **36**, 913–926.

Pesquera, A., Torres-Ruiz, J., Gil-Crespo, P.P. and Velilla, N. (1999) Chemistry and genetic implications of tourmaline and Li-F-Cs micas from the Valdeflores area (C<ceres, Spain). *American Mineralogist*, **84**, 55–69.

Rieder, M. (1970) Chemical composition and physical properties of lithium-iron micas from the Krušné hory Mts. (Erzgebirge). Part A: Chemical composition. *Contributions to Mineralogy and Petrology*, **27**, 131–158.

Rieder, M. (1971) Stability and physical properties of synthetic lithium-iron micas. *American Mineralogist*, **56**, 256–280.

Rieder, M. (2001) Mineral nomenclature in the mica group: the promise and the reality. *European Journal of Mineralogy*, **13**, 1009–1012.

Rieder, M., Cavazzini, G., D'yakonov, Yu.S., Frank-Kamenetskii, V.A., Gottardi, G., Guggenheim, S., Koval', P.V., Müller, G., Neiva, A.M.R., Radoslovich, E.W., Robert, J.-L., Sassi, F.P., Takeda, H., Weiss, Z. and Wones, D.R. (1998) Nomenclature of the micas. *The Canadian Mineralogist*, **36**, 905–912.

Schaller, W.T., Carron, M.K. and Fleischer, M. (1967) Ephesite, $Na(LiAl_2)(Al_2Si_2)O_{10}(OH)_2$, a trioctahedral member of the margarite group, and related brittle micas. *American Mineralogist*, **52**, 1689–1696.

Schmidt, M.W., Dugnani, M. and Artioli, G. (2001) Synthesis and characterization of white micas in the join muscovite-aluminoceladonite. *American Mineralogist*, **86**, 555–565.

Semenov, E. (2001) Notes on ephesite, terskite, Na-komarovite, ceriopyrochlore-(Ce), joaquinite-(Ce) and other minerals from the Ilímaussaq alkaline complex, South Greenland. *Geology of Greenland Survey Bulletin*, **190**, 123–125.

Semenov, E.I. and Shmakin, B.M. (1988) On the composition of mica rocks in exocontacts of rare-metal pegmatites from the Bastar area (India). *Doklady Akademii Nauk SSSR*, **303**, 199–202 (in Russian).

Sun, S. and Yu, J. (1999) Fe-Li micas: a new approach to the substitution series. *Mineralogical Magazine*, **63**, 933–945.

Sun, S. and Yu, J. (2000) Actual Fe-Li mica series as a series with $?_{VI}$ constant but not with $Al_{IV}$ or $Al_{VI}$. *Mineralogical Magazine*, **64**, 755–775.

Teagle, D.A.H., Alt, J.C., Bach, W., Halliday, A.N. and Erzinger, J. (1996) Alteration of upper oceanic crust in a ridge-flank hydrothermal upflow zone: mineral, chemical, and isotopic constraints from hole 896A. *Proceedings of the Ocean Drilling Program, scientific results*, **148** (J.C. Alt, H. Kinoshita, I.B. Stokking and P.J. Michael, editors), pp. 119–150.

Thompson, J.B. (1982) Composition space: an algebraic and geometric approach. Pp. 1–31 in: *Characterization of Metamorphism through Mineral Equilibria* (J.M. Ferry, editor). Reviews in Mineralogy, **10**, Mineralogical Society of America, Washington, D.C.

Tindle, A.G. and Webb, P.C. (1990) Estimation of lithium contents in trioctahedral micas using microprobe data: application to micas from granitic rocks. *European Journal of Mineralogy*, **2**, 595–610.

Tischendorf, G., Gottesmann, B., Förster, H.-J. and Trumbull, R.B. (1997) On Li-bearing micas: estimating Li from electron microprobe analysis and an improved diagram for graphical representation. *Mineralogical Magazine*, **61**, 809–834.

Tischendorf, G., Förster, H.-J. and Gottesmann, B. (1999) The correlation between lithium and magnesium in trioctahedral micas: Improved equations for $Li_2O$ estimation from MgO data. *Mineralogical Magazine*, **63**, 57–74.

Tischendorf, G., Förster, H.-J. and Gottesmann, B. (2001*a*) Minor- and trace-element composition of trioctahedral micas: a review. *Mineralogical Magazine*, **65**, 249–76.

Tischendorf, G., Förster, H.-J. and Gottesmann, B. (2001*b*) Tri- und dioktaedrische Glimmer: ein komplexes chemisches System. *Zeitschrift für Geologische Wissenschaften*, **29**, 275–298.

Tröger, W.E. (1962) Über Protholithionit und Zinnwaldit – Ein Beitrag zur Kenntnis von Chemismus und Optik der Lithiumglimmer. *Beiträge zur Mineralogie und Petrologie*, **8**, 418–431.

Ukai, Y., Nishimura, S. and Hashimoto, Y. (1956)

Chemical studies of lithium micas from the pegmatite of Minagi, Okayama Prefecture. *Mineralogical Journal*, **2**, 27–38.

Wise, W.S. and Eugster, H.P. (1964) Celadonite: Synthesis, thermal stability and occurrence. *American Mineralogist*, **49**, 1032–1083.

Yavuz, F. (2001) LIMICA: a program for estimating Li from electron-microprobe mica analyses and classifying trioctahedral micas in terms of composition and octahedral site occupancy. *Computers & Geosciences*, **27**, 215–227.

Yavuz, F. (2003*a*) Evaluating micas in petrologic and metallogenic aspects: Part I – Definitions and structure of the computer program MICA$^{+}$. *Computers & Geosciences*, **29**, 1203–1213.

Yavuz, F. (2003*b*) Evaluating micas in petrologic and metallogenic aspects: Part II –Applications using the computer program MICA$^{+}$. *Computers & Geosciences*, **29**, 1215–1228.

Zhang, M., Suddaby, P., Thompson, R.N. and Dungan, M.A. (1993) Barian titanian phlogopite from potassic lavas in northeast China: Chemistry, substitutions, and paragenesis. *American Mineralogist*, **78**, 1056–1065.

[*Manuscript received 19 May 2003: revised 20 May 2004*]

# APPENDIX

*Estimation of Li by correlation*

If not measured, the Li content of common K micas may be estimated by considering the correlation relationships of Li with other elements such as Si, Mg, F and Rb (Tindle and Webb, 1990; Tischendorf *et al*., 1997, 1999). In the following, empirical equations are listed, which appear to provide the best results for K micas excluding the celadonite group (all oxides and fluorine are in weight per cent):

*1. Common K micas ›3 MgO*

1.1 Calc-alkaline to peraluminous I- and S-type granitoids; phlogopite, biotite, siderophyllite:

$Li_2O = [2.1/(0.356 + MgO)] - 0.088$,

1.2 Metaluminous to weakly peraluminous granitoids of A-type affinity; Fe-rich biotite, Fe-rich siderophyllite:

$Li_2O = [0.9/(0.26 + MgO)] - 0.05$,

1.3 Alkaline to peralkaline A-type granitoids; annite:

$Li_2O = [0.25/(0.25 + MgO)] - 0.03$,

1.4 Peraluminous magmatic rocks and Mg-enriched environment of crystallization; Al-rich siderophyllite:

$Li_2O = [50.3/(6.5 + MgO)] - 1.54$,

1.5 Alkaline to peralkaline magmatic rocks and Li-Mg-enriched environment of crystallization; tainiolite:

$Li_2O = [98/(12.8 + MgO)] - 0.3$.

*2. Common K micas ‹3 MgO*

2.1 Micas with $Al_2O_3$ <26 and F >4; siderophyllite, zinnwaldite, lepidolite:

$Li_2O = (0.289*SiO_2) - 9.658$,

2.2 Micas with $Al_2O_3$ >26 and F <4; muscovite, phengite:

$Li_2O = 0.3935 \times F^{1.326}$.